High-pressure structural phase transition in $MnWO_4$

J. Ruiz-Fuertes,[1,*] A. Friedrich,[1] O. Gomis,[2] D. Errandonea,[3] W. Morgenroth,[1] J. A. Sans,[4] and D. Santamaría-Pérez[3,5]

[1]*Institut für Geowissenschaften, Goethe-Universität, Altenhöferallee 1, D-60438 Frankfurt am Main, Germany*

[2]*Centro de Tecnologías Físicas, Universitat Politècnica de València, E-46022 Valencia, Spain*

[3]*Departamento de Física Aplicada-ICMUV, Universitat de València, E-46100 Burjassot, Valencia, Spain*

[4]*Instituto de Diseño y Fabricación, Universitat Politècnica de València, E-46022 Valencia, Spain*

[5]*Earth Sciences Department, University College London, Gower Street WC1E 6BT, London, United Kingdom*

(Received 3 November 2014; revised manuscript received 12 March 2015; published 30 March 2015)

The pressure-induced phase transition of the multiferroic manganese tungstate $MnWO_4$ is studied on single crystals using synchrotron x-ray diffraction and Raman spectroscopy. We observe the monoclinic $P2/c$ to triclinic $P\bar{1}$ phase transition at 20.1 GPa and get insight on the phase transition mechanism from the appearance of tilted triclinic domains. Selective Raman spectroscopy experiments with single crystals have shown that the onset of the phase transition occurs 5 GPa below the previously reported pressure obtained from experiments performed with powder samples.

DOI: 10.1103/PhysRevB.91.104109 PACS number(s): 61.50.Ks, 62.50.−p, 75.85.+t, 78.30.Na

I. INTRODUCTION

The prospect of doubling the present data storage density by the simultaneous use of magnetic and electric ordering control has revolutionized the field of multiferroic materials [1]. The potential to control the magnetic order of $MnWO_4$ at constant temperature has turned this material into an ideal candidate for memory devices [2].

$MnWO_4$ crystallizes in a wolframite-type structure [3] with space group $P2/c$, where both Mn and W cations are octahedrally coordinated sharing edges and forming alternating chains of WO_6 and MnO_6 octahedra along the [001] direction (Fig. 1).

$MnWO_4$, with a frustrated magnetic structure below the Néel temperature of 13.7 K, presents up to three different antiferromagnetic (AF) structures with an incommensurate multiferroic phase (AF2) between 12.7 and 7.6 K [4–11]. Unfortunately, the applicability of the multiferroic properties of $MnWO_4$ is constrained to the low temperatures at which the magnetic order takes place. It was shown that the temperature of the AF1 phase (below 7.6 K at ambient pressure) raises at 2.1(1) K/GPa while the AF2 phase is frustrated beyond 4 GPa [12]. Hence, one could speculate that upon sufficient compression the AF1 phase could be stabilized at temperatures closer to room temperature than a few tenths of Kelvin degrees. The structural [13] and optical properties [14] of $MnWO_4$ were studied up to 13.6 GPa, while its vibrational properties were studied up to 39 GPa using Raman spectroscopy and powder samples [15,16]. These studies have shown a high-pressure phase transition and a large influence of the hydrostaticity on the transition pressure, which is 25.7 GPa using Ne as the pressure-transmitting medium (PTM) [15] and at ∼9 GPa lower pressure (17 GPa) without PTM [16]. The dependence of the structural behavior on the presence of deviatoric stresses has already been observed in other nonmagnetic wolframites [17,18]. $ZnWO_4$ and $MgWO_4$ have been found to transform to a $CuWO_4$-type triclinic structure ($P\bar{1}$) at around 17 GPa on high-pressure (HP) powder x-ray diffraction (PXRD) experiments performed under nonhydrostatic conditions (silicone oil) [19] and at around 30 GPa on Raman spectroscopy experiments carried out using Ne as PTM [15]. *Ab initio* calculations on nonmagnetic wolframites $ZnWO_4$ and $MgWO_4$ [19,20] show that the $CuWO_4$-type triclinic phase is energetically competitive with the low-pressure (LP) monoclinic wolframite phase from 1 atm to around 40 GPa. At this pressure, the monoclinic β-fergusonite phase is predicted to be more favorable. However, this phase has not been observed with PXRD so far. In this study we solve the question about the HP phase of $MnWO_4$ performing hydrostatic (Ne) powder x-ray diffraction (PXRD), single-crystal x-ray diffraction (SXRD), and single-crystal Raman spectroscopy up to 31.0 GPa.

II. EXPERIMENTAL DETAILS

HP experiments were carried out using Boehler-Almax diamond-anvil cells (DACs) equipped with conical diamonds of 350-μm culet sizes [21]. Single-crystal and powder samples were obtained from single crystals of 1 mm^3 in size grown by the high-temperature solution method [22]. Samples were loaded together with ruby chips for pressure determination [23] and neon as a quasihydrostatic PTM in order to minimize deviatoric stresses [24] into holes of 130-μm diameter in tungsten gaskets indented to ∼40 μm in thickness. The equation of state (EOS) of Ne was used to confirm the pressure in the PXRD experiments [25]. We performed synchrotron PXRD experiments at the ID15 beamline at Diamond ($\lambda = 0.4246$ Å) up to 19.9 GPa and at the Extreme Conditions Beamline (ECB) at PETRA III ($\lambda = 0.2907$ Å) up to 20.2 GPa. The detector, working distance, and beam size full width at half maximum (FWHM) for the Diamond (run1) and PETRA III (run2) experiments were a MAR345 image plate, 350 mm, 30 × 30 μm^2, and a PerkinElmer XRD 1621 flat-panel detector, 1200 mm, 5 × 5 μm^2, respectively. FIT2D [26] was used to integrate the diffraction patterns, Bragg reflections were indexed with UNITCELL [27], and GSAS [28,29] was employed to carry out the Le Bail refinements [30]. The SXRD experiment was performed at the ECB at PETRA III ($\lambda = 0.2907$ Å) using the same detector as in run2 but with a beam size of 2.4 × 2.1 μm^2 (FWHM) and a detector to sample distance of 400 mm. The diffraction images were collected by 1° ω-scanning. The image

*ruiz-fuertes@kristall.uni-frankfurt.de

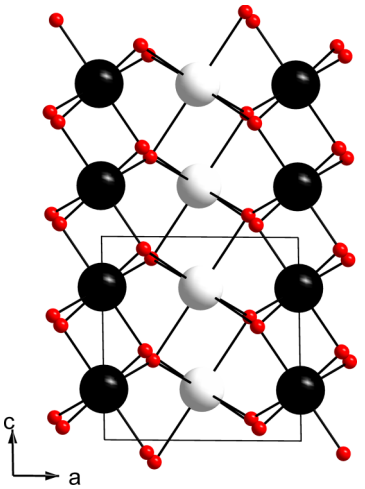

FIG. 1. (Color online) Projection of the structure of the $MnWO_4$ wolframite along [010]. It shows the alternating chains of WO_6 and MnO_6 octahedra. The black (white) spheres represent the W(Mn) atoms.

format was converted according to the procedure described by Rothkirch *et al.* [31] for further processing with the CRYSALIS^{Pro} software [32] for indexing reflections, intensity data reduction, and absorption correction. Crystal structures at 2.4, 14.4, and 20.1 GPa were refined with SHELX97-2 [33] (Supplemental Material) [34]. At higher pressures the decreasing quality of the reflections due to the phase transition prevented refinement of the crystal structure and only indexing of the twin domains was possible. Raman experiments were performed in the backscattering configuration with a Renishaw spectrometer equipped with a 1800 grooves/mm grating. The excitation source was a HeNe laser ($\lambda = 633$ nm) focused down to a 10-μm spot with a 20× long working distance objective and filtered with a notch filter that let us measure above 100 cm^{-1}. The resolution was around 2 cm^{-1}.

III. RESULTS AND DISCUSSION

In Fig. 2 we show the SXRD loading at different selected pressures. As pressure increases the color changes from light brown (2.4 GPa) to red (20.1 GPa) and finally black above 31.0 GPa. Considering the band gap coefficient previously obtained up to 10 GPa in $MnWO_4$ (-22.2 meV/GPa) [14], and making an extrapolation to higher pressures, the band gap at 31 GPa should be around 1.8 eV which corresponds to a wavelength (∼689 nm) that is in the visible range of the electromagnetic spectrum. Taking into account that our sample at 31.0 GPa is black, this indicates a possible band gap collapse probably due to an electronic structure change implied by the structural phase transition. However, this discussion is beyond the scope of this work and should be specifically addressed once the structural and vibrational behavior of $MnWO_4$ had been understood, as we intend in this work. It is interesting to note that optically no formation of domains is observed and that the color change is smooth across the phase transition that takes place at 20.1 GPa as we shall discuss in the next section. Under decompression the sample recovers its initial color as indicative of the reversibility of the phase transition.

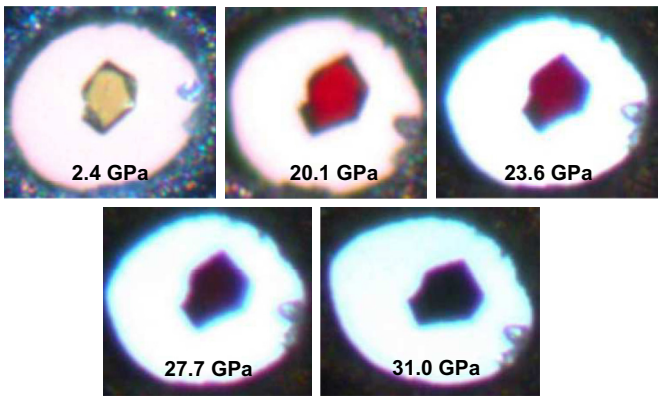

FIG. 2. (Color online) $MnWO_4$ pressurized crystal used in the SXRD experiment at different pressures from ambient pressure to 31.0 GPa.

A. X-ray diffraction: Phase transition

The PXRD experiments were carried out up to a maximum pressure of 20.2 GPa. In run1 the maximum pressure achieved (19.9 GPa) was below the phase transition and therefore we shall focus our discussion on run2. The results for run2 are shown in Fig. 3. The behavior found in run1 is identical to run2 up to 19.9 GPa.

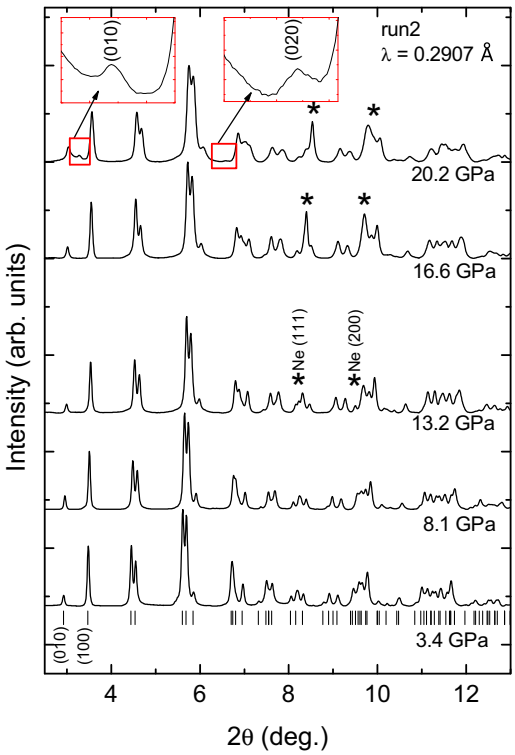

FIG. 3. (Color online) Selection of five diffraction patterns of $MnWO_4$ measured in run2 at different pressures. Vertical bars at 3.4 GPa denote the positions of the Bragg reflections for the $P2/c$ low-pressure phase. The asterisks denote the (111) and (200) reflections of solid Ne. The insets show enlarged areas of the diffraction patterns at 20.2 GPa to illustrate the appearance of weak reflections attributed to the high-pressure phase.

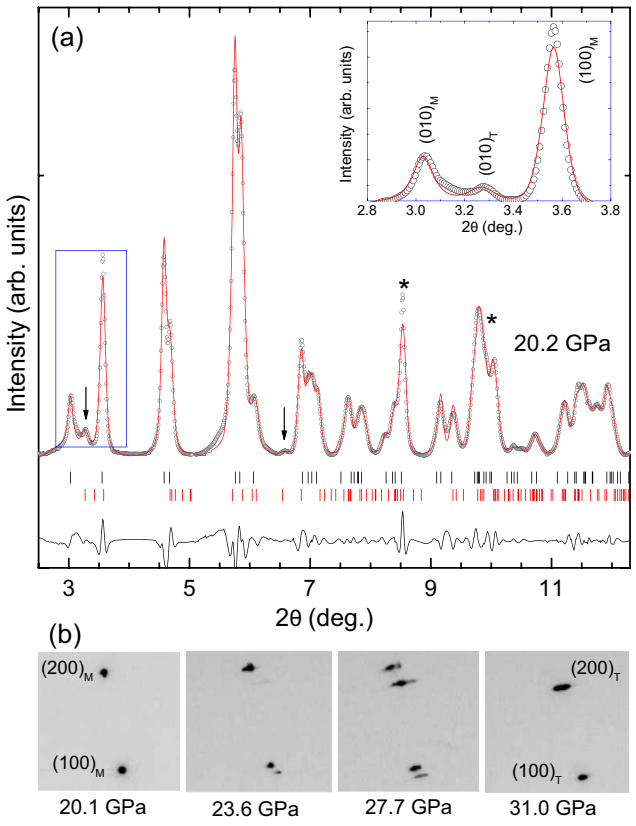

FIG. 4. (Color online) (a) The PXRD diffractogram of $MnWO_4$ at 20.2 GPa (circles) is shown together with a LeBail refinement considering both the LP monoclinic and the HP triclinic phases. The black ticks correspond to the positions of the reflections of the monoclinic phase and the red ones to those of the triclinic phase. The two triclinic reflections observed at this pressure are pointed out by arrows. The asterisks indicate the positions of the Ne reflections. The inset shows the triclinic $(010)_T$ reflection. (b) Pressure evolution of the SXRD measured $(100)_M$ and $(200)_M$ monoclinic Bragg reflections showing the appearance of the $(100)_T$ and $(200)_T$ reflections of the HP triclinic phase up to the complete phase transformation.

Below 20.2 GPa all reflections can be indexed by the LP monoclinic structure. At 20.2 GPa two additional Bragg reflections start to emerge. These two additional reflections are located at $2\theta = 3.2^\circ$ between the $(010)_M$ and the $(100)_M$ monoclinic reflections, and also at $2\theta = 6.6^\circ$, as shown in the insets of Fig. 3. At 20.2 GPa the LP monoclinic phase is still dominant, however, if we compare with previous HP PXRD studies in other wolframites where the phase transition takes place at around 17 GPa, the emergence of the two additional reflections seen in $MnWO_4$ at 20.2 GPa correlates well with the onset of a phase transition [19] to a $CuWO_4$-type triclinic structure ($P\bar{1}$). Here we show that $MnWO_4$ undergoes the same transformation at 20.2 GPa. The Le Bail refinement at 20.2 GPa is reported in Fig. 4(a).

While the Le Bail refinement of the monoclinic phase is reliable at 20.2 GPa, this is not the case for indexing and refinement of the triclinic phase due to its small proportion, low symmetry, and strong reflection overlap. SXRD experiments allow to distinguish between the different phases even for small amounts and to index separately, showing that SXRD experiments are required to solve this phase transition. For this reason, in order to carry out the Le Bail refinement at 20.2 GPa we employed the triclinic metric obtained from the SXRD experiment at 20.1 GPa as starting values. We note that, as commented before, the obtained triclinic cell parameters from the PXRD diffractogram at 20.2 GPa are compromised by the reflection overlap, low symmetry, and small proportion of transited samples at this pressure. The obtained cell parameters at 20.2 GPa from PXRD, and at 2.4, 14.4, 20.1, 23.6, 27.7, and 31.0 GPa from the SXRD experiments are shown in Table I. With PXRD we observe an 8% volume collapse at the phase transition at 20.2 GPa, but since the obtained triclinic cell parameters might be not reliable we shall focus on discussing the SXRD results. With SXRD the phase transition involves a volume collapse of only 1% at 20.1 GPa. However, when the phase transition is complete, the b cell parameter drops from ~5.42 Å at 23.6 GPa to ~5.02 Å, involving a volume collapse. This indicates that the unit-cell parameters obtained from SXRD of the HP triclinic phase are also compromised by the coexistence of the LP and HP phases. At 27.7 GPa we almost do not find reflections from the LP phase, but the reflections of the triclinic phase broaden making their indexing difficult. Therefore, the error bars might be underestimated. The large scattering found for the lattice parameters of the HP phase above 23.6 GPa seems to be a consequence of a large change of the triclinic β angle between these two pressures. In the SXRD experiment we used a sample oriented in the (010) plane (cleavage plane). Therefore, the $(010)_M$ reflection could not be measured. For this reason, we show the evolution of the monoclinic $(100)_M$ and $(200)_M$ and the respective triclinic reflections obtained with SXRD at different pressures in Fig. 4(b). While other triclinic reflections indicate that the phase transition has started already at 20.1 GPa (Fig. 5), the triclinic $(100)_T$ emerges at 23.6 GPa and is accompanied by the triclinic $(200)_T$ reflection at 27.7 GPa with the monoclinic reflections being still present [Fig. 4(b)]. This indicates that both phases coexist below 31 GPa, when the phase transformation to the triclinic phase is completed, confirming that wolframites, and in particular $MnWO_4$, undergo only one phase transformation in hydrostatic conditions in the studied stability range, as observed by Raman spectroscopy [15]. The end of the phase transition obtained with SXRD agrees with the result observed with Raman spectroscopy on powder samples [15], whereas the onset of the transformation is detected 5 GPa before with SXRD. This question will be addressed in detail in the Raman spectroscopy section.

On the left side of Fig. 5 we show the pressure evolution and indexing of a section of one of the 74 SXRD frames of $MnWO_4$ measured at different pressures. The corresponding projection of the obtained reciprocal space along a^* is shown on the right side of Fig. 5. At 14.5 GPa only the monoclinic $(h\bar{1}5)_M$ reflections are observed on the frame section and the high quality of the crystal is reflected in the low dispersion of the reflections along the a^* axis of the reciprocal lattice. At 20.1 GPa the triclinic $(h\overline{41})_{T1}$ reflections start to emerge on the frame section as the result of the onset of the phase transition. Additional weak reflections are observed, which are identified at 23.6 GPa as the $(1\bar{5}0)_{T2}$ reflection and $(h\bar{3}0)_{T2}$ reflections of a second triclinic cell with the same unit-cell parameters as T1. In the reciprocal space we can see that the

TABLE I. Structural parameters of the triclinic and monoclinic structures of $MnWO_4$ at different pressures obtained from the powder and single-crystal x-ray diffraction experiments performed in this work.

	Powder		Single crystal							
Space group	$P2/c$	$P\bar{1}$	$P2/c$	$P2/c$	$P2/c$	$P\bar{1}$	$P2/c$	$P\bar{1}$	$P\bar{1}$	$P\bar{1}$
P (GPa)	20.2(2)	20.2(2)	2.4(1)	14.4(1)	20.1(2)	20.1(2)	23.6(2)	23.6(2)	27.7(2)	31.0(2)
a (Å)	4.674(2)	4.668(3)	4.7983(5)	4.6888(6)	4.6644(7)	4.6725(8)	4.6696(14)	4.664(3)	4.696(3)	4.642(2)
b (Å)	5.499(2)	5.1039(12)	5.708(5)	5.536(6)	5.468(6)	5.4641(17)	5.451(9)	5.419(5)	5.019(2)	5.052(3)
c (Å)	4.8526(19)	4.878(2)	4.9747(5)	4.8844(5)	4.8614(6)	4.816(6)	4.8580(11)	4.780(10)	4.867(6)	4.795(8)
α (deg.)	90	90.80(2)	90	90	90	90.08(5)	90	91.20(10)	92.06(6)	91.8(9)
β (deg.)	91.34(5)	92.32(5)	91.124(7)	91.415(7)	91.603(8)	91.39(4)	91.884(2)	91.00(10)	96.96(9)	97.14(8)
γ (deg.)	90	93.74(3)	90	90	90	90.13(2)	90	90.24(6)	91.33(4)	91.28(4)
V (Å^3)	124.72(13)	116.36(19)	136.23(13)	126.74(14)	123.94(14)	122.91(16)	123.6(2)	120.7(3)	113.76(16)	111.5(2)

quality of the data worsens on pressure increase as the result of the phase transition, and also that the triclinic b^* and c^* axes are tilted in different ways with respect to the monoclinic ones (Fig. 5). On further pressure increase to 27.7 and 31.0 GPa the data quality worsens and most reflections broaden so that diffraction images show a strongly textured powder pattern at 31.0 GPa and cannot be indexed as single crystals anymore. This indicates that the sample does not completely survive the phase transition as a single crystal. The quality of the data does not allow one to determine and refine the crystal structure of the HP triclinic phase which consists of at least two triclinic domains rotated 84° (T1) and −84° (T2) around a^* with respect to the monoclinic cell.

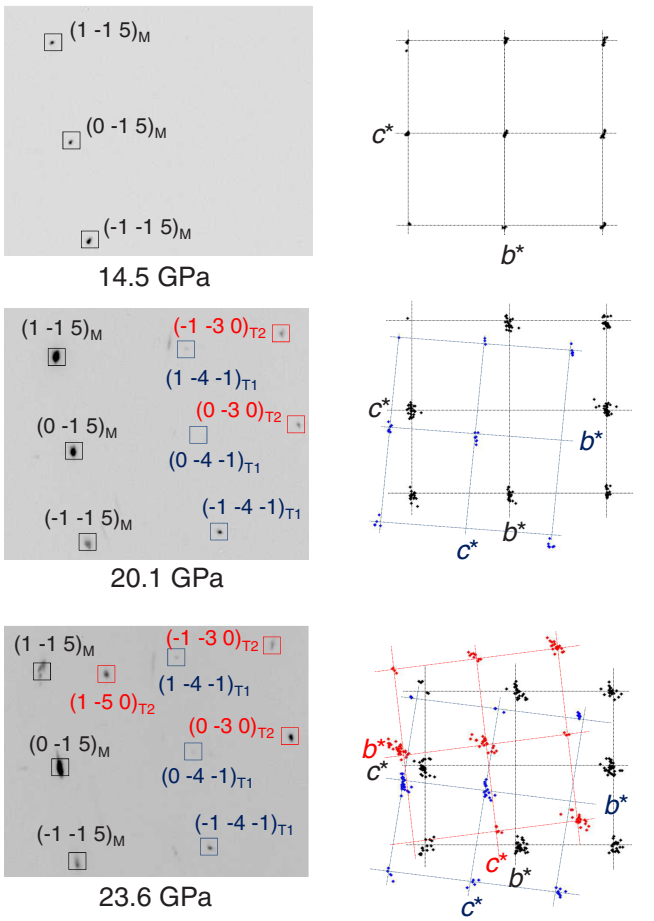

FIG. 5. (Color online) Section of a SXRD frame of $MnWO_4$ measured at different pressures (left) showing the emergence of the reflections of two HP triclinic domains (T1, T2) along the monoclinic (M) one. The corresponding projection of the reciprocal space on the (b^*,c^*) plane (right) is shown at the three selected pressures. The dots represent the location of the measured reflections projected along the a^* axis. The axes of the unit cells are shown as dashed lines. The monoclinic reflections are in black while the triclinic reflections of the two domains are in blue (T1) and red (T2).

B. X-ray diffraction: Compressibility of the LP Phase

Figure 6 shows the pressure dependence of the lattice parameters for the complete stability range of the wolframite phase. Our PXRD and SXRD data overlap well with previous SXRD data up to 9 GPa [13] performed using methanol-ethanol as PTM. However, our PXRD data up to 20.2 GPa can be better explained by a third-order Birch-Murgnahan (BM) EOS than by a second-order BM EOS, despite that SXRD data are well explained with the second-order EOS reported by Macavei and Schulz [13]. The obtained bulk modulus, first derivative, and ambient pressure unit-cell volume obtained from our fit including all PXRD and SXRD data are $B_0 =$ 145(3) GPa, $B_0' = 4.3(2)$, and $V_0 = 138.8(2)$ Å, respectively. This bulk modulus is 9% larger than that obtained by Macavei and Schulz [13] up to 9 GPa with SXRD ($B_0 = 131(2)$ GPa). The axial compressibilities k_x, where x stands for a, b or c lattice parameters, have been obtained from the PXRD and SXRD data using a third-order BM EOS fit considering a pseudocubic cell with volume $V = x^3$ as $k_x = -\frac{1}{3B_0}$ [35]. This is a reasonable approximation since the monoclinic angle $\beta \sim 90°$. For the fit B_0' has been kept fixed to 4.3 to be consistent with the EOS fit. Both a and c lattice parameters account for most of the incompressibility of the unit cell [$k_a = -2.0(1)\times\ 10^{-3}$ and $k_c = -1.6(1)\times 10^{-3}$ GPa^{-1}], whereas the longest axis b is up to two times more compressible [$k_b = -3.3(1)\times 10^{-3}$ GPa^{-1}]. This result is in agreement with the axial compressibilities of other wolframites [19,20] and agrees well with those reported by Macavei and Schulz [13] for $MnWO_4$ up to 9 GPa. It is also worth noting that as pressure increases the monoclinic structure distorts. This can be deduced from the increase of the monoclinic β angle [Fig. 6(b)].

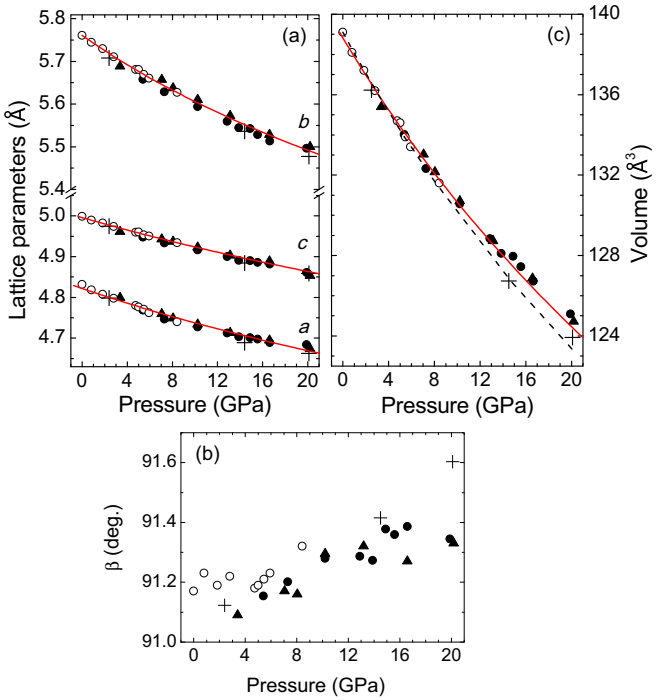

FIG. 6. (Color online) Pressure dependence of the (a) unit-cell lattice parameters (b) monoclinic β angle and (c) volume of $MnWO_4$ in the stability range of the low pressure monoclinic phase. Empty circles represent Macavei and Schulz [13] data while full circles and triangles represent our PXRD data obtained from runs 1 and 2, respectively. The crosses are from our SXRD experiment. The continuous red lines represent the fits to the third-order Birch-Murnaghan equation of state using all available data. The dashed black line represents the equation of state obtained by Macavei and Schulz [13].

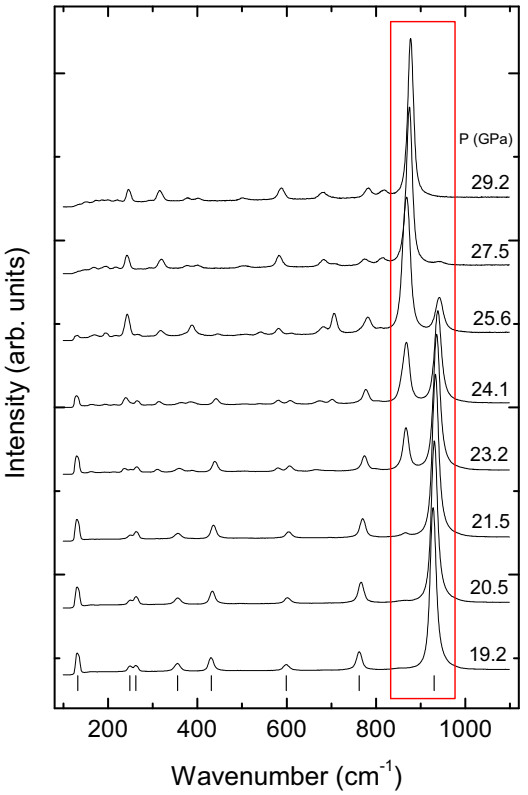

FIG. 7. (Color online) Raman spectra of $MnWO_4$ recorded at selected pressures. The ticks indicate the 8 A_g modes assignation accessed in (010) oriented wolframites in backscattering configuration. At 20.5 GPa, the emergence of an additional Raman active mode at 866 cm^{-1} indicates the onset of the phase transition to the triclinic phase. The region of interest is highlighted with the red box.

C. Raman spectroscopy

Raman spectroscopy is a sensitive technique to observe local structural changes. For this reason, with Raman spectroscopy the detection of the onset of phase transitions is usually observed at lower pressures than with XRD which needs larger amounts of the transited sample to detect the onset. In a previous HP Raman spectroscopy work performed with powder samples and Ne as PTM [15], the onset of the phase transition of $MnWO_4$ was determined at 25.7 GPa. However, using the same experimental conditions our present PXRD has shown the emergence of reflections of the triclinic phase at 20.2 GPa.

In wolframites there are 8 A_g and 10 B_g Raman active modes, while in the $CuWO_4$-type triclinic phase there are 18 A_g modes. The B_g mode with the highest frequency (774 cm^{-1} at 1 atm in $MnWO_4$), is broad and presents a large pressure coefficient (3.58 cm^{-1} GPa^{-1}) [15]. The onset of the phase transition of wolframites is observed by the appearance of the highest frequency A_g triclinic mode. This mode, which is the most intense of the HP phase, emerges in the frequency region of the highest frequency B_g broad mode of the LP phase. Although the triclinic mode grows fast in intensity, the coincidence in frequency with the broad B_g mode might explain a detection delay of the onset of the phase transition with respect to XRD. In order to demonstrate that this is the case we have performed Raman spectroscopy measurements on oriented single crystals at HP. The Raman tensors of the two monoclinic modes are

$$A_g = \begin{pmatrix} a & 0 & d \\ 0 & b & 0 \\ d & 0 & c \end{pmatrix}, \quad B_g = \begin{pmatrix} 0 & e & 0 \\ e & 0 & f \\ 0 & f & 0 \end{pmatrix}.$$

Wolframites exfoliate in the (010) plane facilitating the use of tiny and high-quality oriented samples appropriate to be loaded in the DAC. As derived from the Raman tensors, in backscattering geometry and with (010) oriented samples, the B_g modes scatter light polarized along the collection direction [010] and therefore cannot be detected, while the A_g modes, scattering light polarized along the sample [100] and [001] directions are always detected for this configuration [22,36]. Although the pressurized diamonds in a DAC have an unpolarizing effect, we have only accessed the 8 A_g modes in backscattering unpolarized Raman experiments with a (010)-oriented sample with an unpolarized excitation source (Fig. 7). Similarly to experiments performed with powders [15], all A_g modes shift to higher frequencies as pressure increases. However, now that the LP monoclinic B_g modes are not present, the emergence of the highest frequency A_g triclinic mode is detected at 20.5 GPa in good agreement with our PXRD and SXRD.

IV. CONCLUSIONS

The structural stability of multiferroic $MnWO_4$ wolframite has been studied using powder x-ray diffraction up to 20.2 GPa and single crystal x-ray diffraction up to 31.0 GPa. We have shown that $MnWO_4$ undergoes only one phase transition up to the maximum studied pressure to a triclinic structure with space group $P\bar{1}$. The onset of the phase transition in hydrostatic conditions is at 20.1 GPa. The indexing performed in the single-crystal XRD experiment has revealed the complex nature of this phase transition with the appearance of two triclinic domains rotated with respect to the parent structure 84° and −84°, respectively, around a^*. The controversy regarding the determination of the onset of the phase transition using Raman spectroscopy has been addressed performing selective Raman spectroscopy in single crystals. The absence of the low-pressure B_g monoclinic modes in (010)-oriented samples in backscattering geometry has allowed us to accurately detect the onset of the phase transition, which occurs 5 GPa below the reported pressure obtained from experiments on powder samples. In summary, in this work it has been determined that the high-pressure phase of multiferroic $MnWO_4$ is triclinic ($P\bar{1}$). Given the symmetry lowering that this phase transition implies one can necessarily expect an effect on the magnetic exchange interactions. In fact, in a similar compound like $CuWO_4$ the reverse phase transition has been predicted to involve an antiferro- to ferromagnetic phase transition [37]. In addition, the stabilization of the incommensurate multiferroic phase of CuO recently has been predicted to be stabilized at ambient temperature with the use of high pressure [38]. According to the pressure coefficient reported by Chaudhury *et al.* [12] for the magnetic phase boundaries of $MnWO_4$, the observed phase transition of $MnWO_4$ to a structure with lower symmetry rules out the possibility of stabilization upon compression of any of these magnetic phases of $MnWO_4$ at ambient temperature.

ACKNOWLEDGMENTS

The authors thank Professor M. M. Gospodinov from the Institute of Solid State Physics of Bulgaria for providing single-crystal samples of $MnWO_4$. This research was partially supported by the Spanish government MINECO under Grant No. MAT2013-46649-C4-1/2-P and by Generalitat Valenciana Grants No. ACOMP-2013-1012 and No. ACOMP-2014-243. We acknowledge Diamond Light Source for time on beamline I15 under proposal EE6517 and I15 beamline scientist for technical support. DESY-Photon Science is gratefully acknowledged. PETRA III at DESY is a member of the Helmholtz Association (HGF). J.R.-F. thanks the Alexander von Humboldt Foundation for a postdoctoral fellowship and T. Bernert from the Max-Planck Institut für Kohlenforschung for fruitful discussions. A.F. acknowledges financial support from the DFG within the priority program SPP1236 (Project No. FR2491/2-1), W.M. acknowledges the BMBF (Projects No. 05K10RFA and No. 05K13RF1), and J.A.S. acknowledges the MINECO for a Juan de la Cierva postdoctoral fellowship.

[1] S. W. Cheong and M. Mostovoy, Nat. Mater. **6**, 13 (2007).
[2] T. Finger, D. Senff, K. Schmalzl, W. Schmidt, L. P. Regnault, P. Becker, L. Bohaty, and M. Braden, Phys. Rev. B **81**, 054430 (2010).
[3] A. W. Sleight, Acta Cryst. B **28**, 2899 (1972).
[4] H. Dachs, H. Weitzel, and E. Stoll, Solid State Commun. **4**, 473 (1966).
[5] H. Dachs, E. Stoll, and H. Weitzel, Z. Kristallogr. **125**, 120 (1967).
[6] G. Lautenschläger, H. Weitzel, T. Vogt, R. Hock, A. Böhm, M. Bonnet, and H. Fuess, Phys. Rev. B **48**, 6087 (1993).
[7] K. Taniguchi, N. Abe, T. Takenobu, Y. Iwasa, and T. Arima, Phys. Rev. Lett. **97**, 097203 (2006).
[8] O. Heyer, N. Hollmann, I. Klassen, S. Jodlauk, L. Bohaty, P. Becker, J. A. Mydosh, T. Lorenz, and D. Khomskii, J. Phys.: Condens. Matter. **18**, L471 (2006).
[9] D. Meier, M. Maringer, T. Lottermoser, P. Becker, L. Bohaty, and M. Fiebig, Phys. Rev. Lett. **102**, 107202 (2009).
[10] I. Urcelay-Olabarria, J. M. Pérez-Mato, J. L. Ribeiro, J. L. García-Muñoz, E. Ressouche, V. Skumryev, and A. A. Mukhin, Phys. Rev. B **87**, 014419 (2013).
[11] H. Nojiri, S. Yoshii, M. Yasui, K. Okada, M. Matsuda, J. S. Jung, T. Kimura, L. Santodonato, G. E. Granroth, K. A. Ross *et al.*, Phys. Rev. Lett. **106**, 237202 (2011).
[12] R. P. Chaudhury, F. Yen, C. R. de la Cruz, B. Lorenz, Y. Q. Wang, Y. Y. Sun, and C. W. Chu, Physica B **403**, 1428 (2008).
[13] J. Macavei and H. Schulz, Z. Kristallogr. **207**, 193 (1993).
[14] J. Ruiz-Fuertes, S. López-Moreno, J. López-Solano, D. Errandonea, A. Segura, R. Lacomba-Perales, A. Muñoz, S. Radescu, P. Rodríguez-Hernández, M. Gospodinov *et al.*, Phys. Rev. B **86**, 125202 (2012).
[15] J. Ruiz-Fuertes, D. Errandonea, O. Gomis, A. Friedrich, and F. J. Manjón, J. Appl. Phys. **115**, 043510 (2014).
[16] R. C. Dai, X. Ding, Z. P. Wang, and Z. M. Zhang, Chem. Phys. Lett. **586**, 76 (2013).
[17] D. Errandonea, F. J. Manjón, N. Garro, P. Rodríguez-Hernández, S. Radescu, A. Mújica, A. Muñoz, and C. Y. Tu, Phys. Rev. B **78**, 054116 (2008).
[18] J. Ruiz-Fuertes, D. Errandonea, S. López-Moreno, J. González, O. Gomis, R. Vilaplana, F. J. Manjón, A. Muñoz, P. Rodríguez-Hernández, A. Friedrich *et al.*, Phys. Rev. B **83**, 214112 (2011).
[19] J. Ruiz-Fuertes, S. López-Moreno, D. Errandonea, J. Pellicer-Porres, R. Lacomba-Perales, A. Segura, P. Rodríguez-Hernández, A. Muñoz, A. H. Romero, and J. González, J. Appl. Phys. **107**, 083506 (2010).
[20] S. López-Moreno, A. H. Romero, P. Rodríguez-Hernńdez, and A. Muñoz, High. Press. Res. **29**, 578 (2009).
[21] R. Boehler, Rev. Sci. Instrum. **77**, 115103 (2006).
[22] M. N. Iliev, M. M. Gospodinov, and A. P. Litvinchuk, Phys. Rev. B **80**, 212302 (2009).
[23] H. K. Mao, J. Xu, and P. M. Bell, J. Geophys. Res. **91**, 4673 (1986).
[24] S. Klotz, J.-C. Chervin, P. Munsch, and G. L. Marchand, J. Phys. D: Appl. Phys. **42**, 075413 (2009).

[25] A. Dewaele, F. Datchi, P. Loubeyre, and M. Mezouar, Phys. Rev. B **77**, 094106 (2008).
[26] A. P. Hammersley, S. O. Svensson, M. Hanfland, A. N. Fitch, and D. Häusermann, High. Press. Res. **14**, 235 (1996).
[27] T. J. B. Holland and S. A. T. Redfern, Mineralog. Mag. **61**, 65 (1997).
[28] A. C. Larson and R. B. Von Dreele, Los Alamos National Laboratory Report LAUR, 86-748 (2000).
[29] B. H. Toby, J. Appl. Cryst. **34**, 210 (2001).
[30] A. Le Bail, Powder Diffr. **20**, 316 (2005).
[31] A. Rothkirch, G. D. Gatta, M. Meyer, S. Merkel, M. Merlini, and H. P. Liermann, J. Synchrotron Rad. **20**, 711 (2013).
[32] Agilent, computer code CRYSALIS^{Pro} software system, Version 1.171.36.28, Agilent Technologies, Oxford, UK, 2013.
[33] G. M. Scheldrick, Acta Crystallogr. A **64**, 112 (2008).
[34] See Supplemental Material at http://link.aps.org/supplemental/10.1103/PhysRevB.91.104109 for the CIF files of the refined structure of wolframite-type $MnWO_4$ at different pressures.
[35] R. J. Angel, *Equations of State*, Vol. 41, High-pressure, High-temperature Crystal Chemistry. Reviews in Mineralogy and Geochemistry (Mineralogical Society of America, Washington, DC, 2001).
[36] E. Kroumova, M. I. Aroyo, J. M. Pérez Mato, A. Kirov, C. Capillas, S. Ivantchev, and H. Wondratç, Phase Trans. **76**, 155 (2003).
[37] J. Ruiz-Fuertes, D. Errandonea, R. Lacomba-Perales, A. Segura, J. González, F. Rodríguez, F. J. Manjón, S. Ray, P. Rodríguez-Hernández, A. Muñoz *et al.*, Phys. Rev. B **81**, 224115 (2010).
[38] X. Rocquefelte, K. Schwarz, P. Blaha, S. Kumar, and J. van den Brink, Nat. Commun. **4**, 2511 (2013).